Nanocrystallinity and Magnetic Property Enhancement in Melt-Spun Iron-Rare Earth-Base Hard Magnetic Alloys

H.A. Davies, A. Manaf, and P.Z. Zhang

Refinement of the grain size below ~35 nm mean diameter in melt-spun FeNdB-base alloys leads to enhancement of remanent polarization, J_r, above the level predicted by the Stoner-Wohlfarth theory for an aggregate of independent, randomly oriented, and uniaxial magnetic particles. This article summarizes the results of the recent systematic research on this phenomenon, including the influence of alloy composition and processing conditions on the crystallite size, degree of enhancement of J_r, and maximum energy product $(BH)_{max}$. It has been shown that the effect can also occur in ternary FeNdB alloys, without the addition of silicon or aluminum, which was originally thought necessary, providing the nanocrystallites are not magnetically decoupled by a paramagnetic second phase. Values of $(BH)_{max}$ above 160 kJ · m^{-3} have been achieved. The relationship between grain size, J_r, intrinsic coercivity, $_JH_C$, and $(BH)_{max}$ are discussed in terms of magnetic exchange coupling, anisotropy, and other parameters. Recent extension of this work to the enhancement of properties in Fe-Mischmetal-Boron-base alloys and to bonded magnets with a nanocrystalline structure is also described.

Keywords
hard magnets, iron-neodymium alloys, magnetic materials, nanocrystallinity

1. Introduction

THE chill-block melt-spinning route for processing iron-neodymium-boron permanent magnet alloys[1,2] is now well established. The ribbon is normally cast to yield a microcrystalline $Fe_{14}Nd_2B$ structure (designated MQ) with a mean grain size of 50 to 60 nm and a random crystallographic orientation. Although the intrinsic coercivity, $_JH_C$, of the alloy in this form is high (~1200 kA · m^{-1}), because each crystallite consists of a single magnetic domain, the values of remanent polarization, J_r (0.8 T), and maximum energy product, $(BH)_{max}$ (up to 112 kJ · m^{-3}), are modest due to the random orientation. Nevertheless, even in its as-cast form, the alloy is a commercially attractive material, because its phase constitution is sufficiently refined and homogeneous that, after crushing to a powder, it can be polymer bonded to chemically stable magnets (designated MQI)[3] with all the advantages of shape flexibility and productivity that this entails.

However, there are substantial economic and technological benefits to be gained from improving the $(BH)_{max}$ of bonded FeNdB magnets. One method that has been developed involves the use of alloy powder feedstock derived by crushing die-upset forged FeNdB magnets (designated MQIII), in which a strong preferred orientation has resulted from the upsetting process.[3] This has been shown to yield good properties, although with the disadvantage of a lengthened process route and increased production costs.[4]

H.A. Davies, A. Manaf, and **P.Z. Zhang,** Department of Engineering Materials, University of Sheffield, Robert Hadfield Building, Mappin Street, Sheffield S1 4DU, United Kingdom.

An interesting alternative approach is to induce enhancement of J_r and $(BH)_{max}$ without introducing crystallographic texture in the ribbon. This phenomenon, in which J_r is enhanced above the theoretically expected value of $J_s/2$, where J_s is the saturation polarization for $Fe_{14}Nd_2B$ (1.6 T), was first reported by Keem et al.[5] for alloys containing silicon or aluminum. It was suggested that the effect was associated with grain refinement down to a mean diameter below ~25 nm and that this was promoted by the silicon or aluminum additions.[6] Similar behavior was also reported by Matsumoto et al.,[7] Hadjipanayis and Gong,[8] and Davies et al.,[9] and by Yajima et al. for small zirconium additions.[10] Also, J_r enhancement was observed in combination with hard magnetic characteristics for a very low neodymium alloy $Fe_{78}Nd_4B_{18}$, in which the major phase was Fe_3B and only 15% of the iron atoms was present as $Fe_{14}Nd_2B$ phase.[11]

Subsequently, present the authors have shown that the remanence enhancement phenomenon appears to be quite general, at least with respect to $Fe_{14}Nd_2B$ alloys, occurring for suitable processing conditions not only for small alloying additions,[12] but also for ternary FeNdB alloys[13] and for alloys based on other rare earth metals such as mischmetal[14] and didymium.[15]

The purpose of this article is to summarize the recent experimental investigations and present knowledge and understanding of the phenomenon and discuss the extent to which it might be exploited commercially for the production of improved magnets.

2. Experimental Procedure

The iron-rare-earth-boron alloys were rapidly solidified as ribbon with thicknesses ranging from ~13 to 50 μm by melt spinning onto a copper roll at circumferential speeds, V_p, of 13 to 50 m · s^{-1} in an argon atmosphere. Quartz crucibles with nozzle diameters of 0.6 mm and a melt propelling pressure of

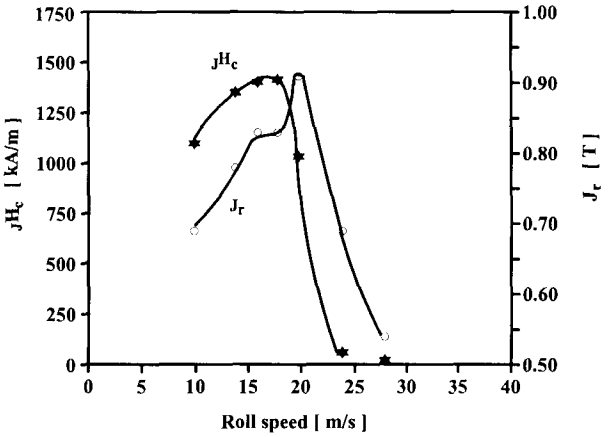

Fig. 1 Dependence of remanence, J_r, and coercivity, $_JH_C$, on roll speed for melt-spun $Fe_{79.6}Nd_{13.2}B_6Si_{1.2}$.

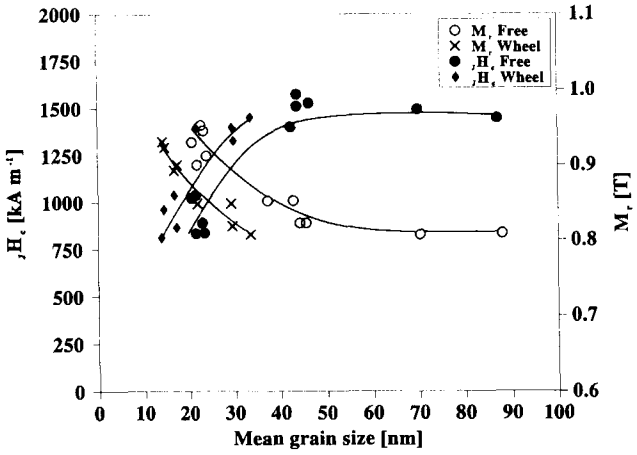

Fig. 2 Dependence of remanence, J_r, and coercivity, $_JH_C$, on grain size dg for melt-spun $Fe_{79.6}Nd_{13.2}B_6Si_{1.2}$.

argon 3.5×10^4 Pa were used. Thicker ribbons cast at a lower V_r were crystalline, and thinner ribbons spun at a higher V_r were noncrystalline, the critical values of t_r and V_r depending on alloy composition. The mean t_r value was determined from measurements at several points on a sample using a digital transducer point-micrometer. The structures and magnetic properties of crystalline ribbon were investigated in the as-cast state, whereas those for initially amorphous ribbons were studied after devitrification annealing at a temperature appropriate to the composition. The mean crystallite size was generally determined by X-ray line broadening analysis using the Scherrer formula after correction for instrumental broadening.[16] In some cases, mean grain sizes were also confirmed by transmission electron microscopy (TEM). X-ray diffraction was also used to monitor the phase constitution and the relative intensities of diffraction peaks.

The *J-H* loops of individual ribbon samples (typical mass ~2 mg) and, in some cases, of magnets fabricated from crushed ribbon were measured with an Oxford Instruments VSM, equipped with a superconducting magnet with a maximum field of 5 T. Measurements were generally made across the ribbon width, i.e., in-plane but perpendicular to the spinning direction. For selected samples, measurements were performed in three orthogonal directions to check for isotropy. Microstructural studies of thin foils, ion-beam thinned from VSM pretested ribbon samples, were performed mainly with a JEOL 200CX transmission electron microscope operating at 200 keV, although some observations also were made with a JEOL HR 2010 instrument.

3. Remanence Enhancement in a Fe-Nd-B-Si Alloy

The alloy $Fe_{79.6}Nd_{13.2}B_6Si_{1.2}$ was chosen for initial detailed study, because it had previously been shown to manifest $J_r > 0.5\ J_s$ by Keem and co-workers.[5] The influence of V_r on $_JH_C$ and J_r for this alloy is shown in Fig. 1. The coercivity increases with increasing V_r up to a maximum value of 1440 kA · m^{-1} (18 kOe) at $V_r = 18$ m · s^{-1}. Correspondingly, the remanence also increases with increasing V_r and levels off at 18 m · s^{-1}. The velocity dependence of $_JH_C$ is similar to that observed for melt-spun ternary Fe-Nd-B alloys by Croat et al.[1] and reflects the initially decreasing grain size with increasing cooling rate, as V_r is increased, and subsequent vitrification at higher V_r, which leads to a steep decline in coercivity.

However, in contrast to the behavior reported by Croat et al., J_r in the present case increases for V_r between 18 and 20 m · s^{-1}, at which value it achieves a maximum of 0.92 T. It then declines with a further increase in V_r. At peak J_r values the ribbons were confirmed to be isotropic from VSM *J-H* loop measurements along the ribbon length, across the width, and through-thickness with no significant difference being found. They were also confirmed as being crystallographically isotropic in-plane from electron diffraction patterns of foils derived from ribbon samples. The magnitude of $(BH)_{max}$ is dominated by J_r at medium and high coercivities, around the peak, and thus, $(BH)_{max}$ has a similar dependence on V_r as does J_r, with a maximum value of 144 kJ · m^{-3} (18 MGOe). The relationship between J_r and V_r is thus more complex than was evident from the initial studies by Croat et al.,[1] where J_r peaked at 0.8 T, consistent with the Stoner-Wohlfarth model for single domain particles[17] and with a corresponding $(BH)_{max}$ of 104 kJ · m^{-3} (13 MGOe). In the present study, J_r and $(BH)_{max}$ clearly exceed the respective values predicted by the Stoner-Wohlfarth model over the range of V_r 18 to 20 m · s^{-1}. Moreover, these curves show that the peak coercivity does not correspond to the initiation of vitrification, but rather this is indicated by the peak J_r.

The enhancement of J_r and attenuation of $_JH_C$ are illustrated clearly in Fig. 2, in which J_r and $_JH_C$ are plotted against the mean grain diameter, d_g, for each of a series of ribbon thicknesses. The value of d_g was determined in each case for a VSM tested ribbon sample. Generally, enhancement of J_r above 0.8 T became significant for $d_g \leq 40$ nm when measured on the noncontact face or ≤30 nm for the roll contact surface. For the latter, d_g was reduced to ~15 nm before vitrification commenced. The difference in mean grain size across the thickness of the ribbons, which appears to be approximately constant with decreasing t_r, indicates an apparently persistent grain size variation from top to bottom, but probably reflects the exist-

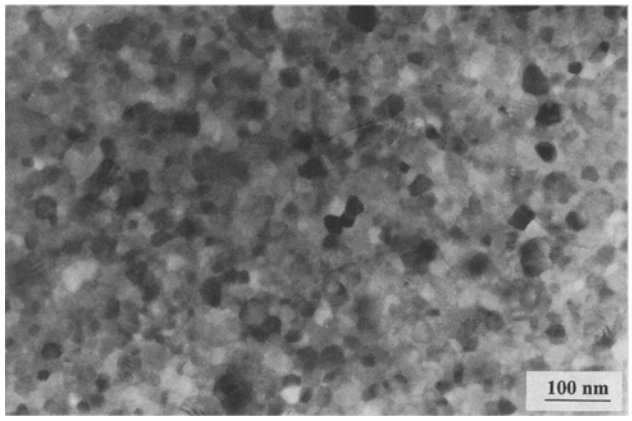

Fig. 3 Transmission electron micrograph of typical nanocrystalline single-phase $Fe_{14}Nd_2B$ grain structure in melt-spun $Fe_{79.6}Nd_{13.2}B_6Si_{1.2}$ ribbon.

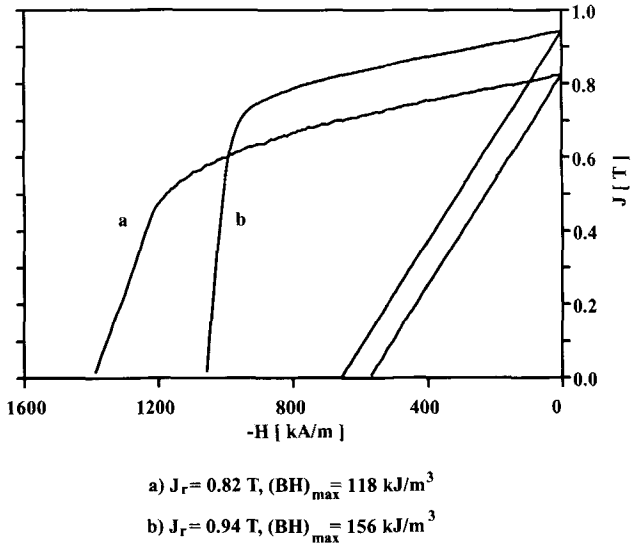

Fig. 4 Second quadrants of *J-H* loops for nanostructured (a) and microcrystalline (b) $Fe_{79.6}Nd_{13.2}B_6Si_{1.2}$ ribbons.

ence of a chill zone formed adjacent to the roll surface for all ribbon thicknesses. This enhancement of J_r is associated with what can be described as a nanocrystalline structure, in which $d_g \leq 30$ nm, and these observations confirm quantitatively the earlier findings of Clemente et al.[6] A transmission electron micrograph of typical single-phase $Fe_{14}Nd_2B$ ultrafine-grained (or nanocrystalline) ribbon with an enhanced J_r is shown in Fig. 3. The second quadrant of the *J-H* loop for this type of ribbon is shown in Fig. 4, with that for a microcrystalline sample with a mean grain size of ~50 nm. The former exhibits increased squareness, which suggests a narrower distribution of grain size in the bulk of the ribbon. It should, however, be emphasized that in all cases the melt-spun ribbons are characterized by periodic cast-in gas pockets on their roll contact surfaces. This leads to a local reduction in cooling rate and a marked increase in grain size in the vicinity of these pockets, although the overall volume fraction of these coarse grains is estimated to be small (<10%).

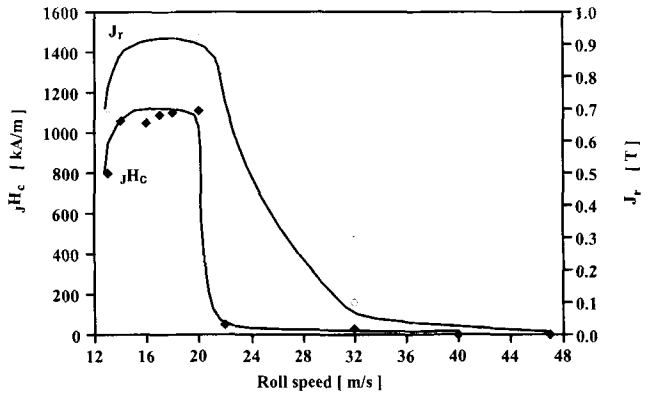

Fig. 5 Dependence of J_r and $_JH_C$ on roll speed for melt-spun low-boron $Fe_{82.4}Nd_{13.1}B_{4.5}$ alloy ribbon.

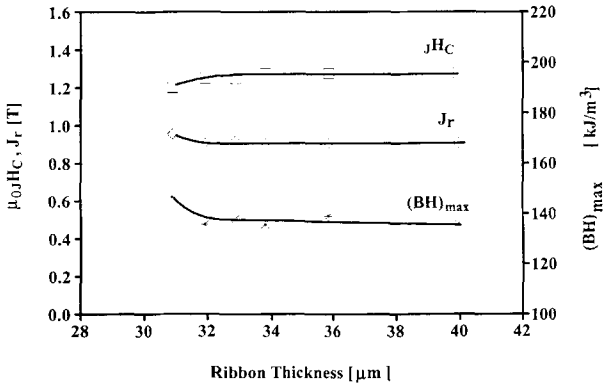

Fig. 6 Dependence of magnetic properties (J_r, $_JH_C$, and $(BH)_{max}$) on ribbon thickness for melt-spun $Fe_{82.4}Nd_{13.1}B_{4.5}$.

4. Remanence Enhancement in Ternary Fe-Nd-B Alloys

In a subsequent study,[13,18] the authors showed that J_r could also be enhanced in a ternary low-boron alloy, $Fe_{82.4}Nd_{13.1}B_{4.5}$. The measured J_r and $_JH_C$ for the as-quenched alloy as functions of V_r are given in Fig. 5. The overall shape of the curves resembles that for conventional microcrystalline Fe-Nd-B alloys,[1] but J_r exceeds 0.8 T (up to 0.92 T), and moreover, this occurs over a wide range of V_r values. In contrast to the Fe-Nd-B-Si alloy described earlier, the coercivity for this alloy does not appear to decrease as the remanence is enhanced. Hence, the optimum properties, which were associated with a mean grain size (measured on the roll contact side) of ~20 nm, represented a particularly favorable combination of J_r of ~0.9 T, $_JH_C$ of ~1100 kA · m^{-1} (13.8 kOe), and $(BH)_{max}$ of ~140 kJ · m^{-3} (17.5 MGOe) over a substantial plateau of process conditions. The relatively lower sensitivity to casting parameters is also emphasized in Fig. 6, in which J_r,

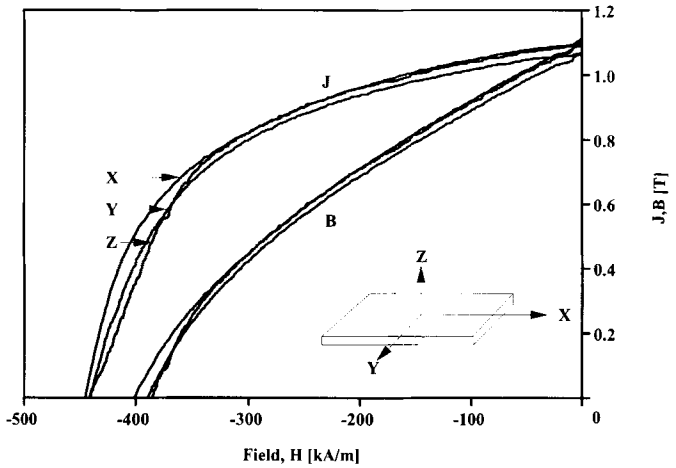

Fig. 7 Second quadrants of *J-H* and *B-H* hysteresis loops for three orthogonal directions (*x*-longitudinal) in a nanostructured ribbon sample of $Fe_{86}Nd_9B_5$.

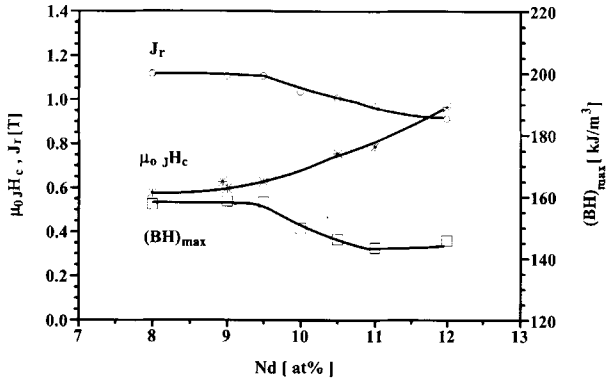

Fig. 8 Magnetic properties of melt-spun ribbon in the thickness range 25 to 34 μm as a function of neodymium content for alloys of composition $Fe_{86-x}Nd_{8+x}B_6$ over the range x = 0 to 4 at.%.

${}_JH_C$, and $(BH)_{max}$ are plotted against ribbon thickness, with all three properties being virtually constant until t_r falls below 32 μm. The processing window for this alloy may be sufficiently wide to facilitate large-scale production by direct quenching.

A particularly interesting feature of this alloy is that it is single phase in the as-quenched nanocrystalline condition, in spite of containing almost 25% less boron than the stoichiometric composition, $Fe_{82.4}Nd_{11.8}B_{5.8}$. This indicates that a considerable degree of nonstoichiometry, at least with respect to the smallest constituent atom, which is boron, can be induced in the $Fe_{14}Nd_2B$ phase by rapid solidification. The metastability was further confirmed by annealing studies, which revealed the precipitation of αFe phase.[13]

The authors have also observed remanence substantially enhanced above the Stoner-Wohlfarth value of 0.8 T for the $Fe_{14}Nd_2B$ phase in nanostructured alloy ribbons having compositions $Fe_{86-x}Nd_{8+x}B_6$ with x = 0 to 4 at.%.[19-21] At x = 4, the composition is very close to stoichiometric $Fe_{14}Nd_2B$, whereas for x = 0, there is about a 30% deficit of neodymium. As the neodymium content is decreased to 8 at.%, the remanence enhancement increases whereas ${}_JH_C$ decreases. The ribbons remained crystallographically and magnetically isotropic in all cases. The latter is illustrated by the second quadrant *J-H* and *B-H* loops for three orthogonal directions in the ribbon, longitudinal, transverse, and plane normal (the last after correction for self-demagnetization), which are given in Fig. 7. No significant difference is observed between these. The properties of the melt-spun ribbons are plotted against neodymium concentration for $V_r = 18\ m \cdot s^{-1}$ in Fig. 8. As shown in Fig. 9, J_r is consistently >0.8 T, even for the near-stoichiometric alloys, and increases to 1.1 T for $Fe_{86}Nd_8B_6$. For neodymium contents of ≤11 at.%, the ribbons become two phase, the $Fe_{14}Nd_2B$ grains (d_g < 30 nm) being interspersed with smaller, isolated grains of αFe, which are typically only ~10 nm wide.[19]

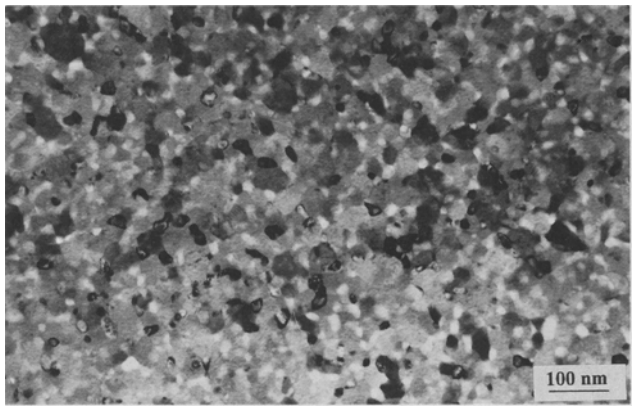

Fig. 9 TEM micrograph of a nanostructured two-phase $Fe_{86}Nd_8B_6$ ribbon showing $Fe_{14}Nd_2B$ grains interspersed with isolated smaller particles of αFe.

The increasing J_r with decreasing neodymium content is accompanied by a lowering of ${}_JH_C$, as was observed for the silicon-containing alloy discussed earlier, but this decrease is relatively gradual, despite the increasing volume fraction of the magnetically soft αFe phase. Evidently, when the soft phase is sufficiently finely distributed, it does not lead to deterioration of the loop shape in the second quadrant and to collapse of the energy product, as would normally be the case in microcrystalline ribbon. This was also observed for the very low neodymium alloy $Fe_{77}Nd_{4.5}B_{18.5}$, studied by Coehoorn and co-workers,[11] for which only some 15% of the iron atoms were present as $Fe_{14}Nd_2B$. The other phases were Fe_3B and αFe. This alloy in devitrified form was nanostructured on an even finer scale than the present compositions.

The values of $(BH)_{max}$ for the highest remanence nanocrystalline ribbons (lower neodymium) are in excess of 160 kJ · m^{-3} (>20 MGOe) or about 50% greater than for isotropic microcrystalline Fe-Nd-B ribbon.[19,20]

5. Neodymium-Rich Ribbons with High Coercivity

The authors investigated several alloy compositions in which the neodymium content is increased to levels well beyond the stoichiometric $Fe_{14}Nd_2B$ concentration, together

with in most cases small additions of other elements such as niobium and dysprosium, which are known to increase coercivity.[122] The common feature of all of these alloys is that they contain a neodymium-rich phase located along the grain boundaries. The second quadrant demagnetization curves for these ribbon samples, which have been spun generally under conditions such as to yield a nanocrystalline structure, are given in Fig. 10. It is evident that, as the concentration of neodymium and solute elements increases, the intrinsic coercivity also increases, and in this present series, a peak value of 2240 kA · m^{-1} (28 kOe) was observed for the alloy. J_r does not exceed 0.8 T and indeed decreases progressively to 0.6 T for the highest total (neodymium + solute) concentration, due to the large volume dilution of the $Fe_{14}Nd_2B$ by the paramagnetic, neodymium-rich phase. Hence, it is apparent that, when the $Fe_{14}Nd_2B$ grains are decoupled by a paramagnetic phase, a nanostructure no longer promotes remanence enhancement.

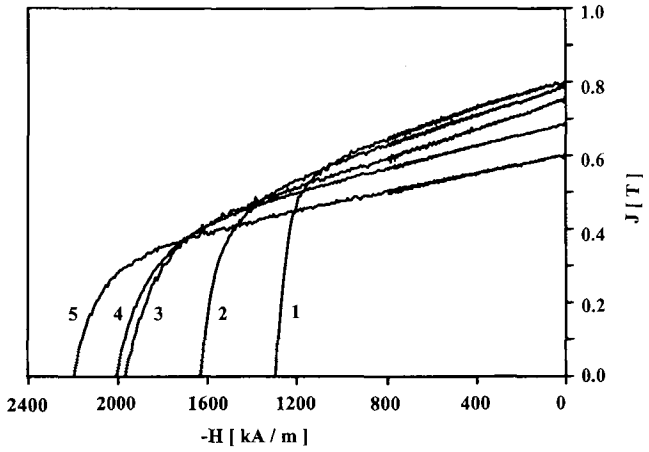

Fig. 10 Second quadrant demagnetization curves for several neodymium-rich alloys showing enhanced coercivity. (1) $Fe_{78}Nd_{14.3}B_{7.7}$. (2) $Fe_{76}Nd_{16}B_7Nb_1$. (3) $Fe_{76}Nd_{14.5}Dy_{1.5}B_7Nb_1$. (4) $Fe_{73.8}Nd_{19.5}B_{6.2}Si_{0.5}$. (5) $Fe_{73}Nd_{18}Dy_{1.5}B_6Si_{0.5}Nb_1$.

6. Alloys Based on Mischmetal and Didymium

Mischmetal is a mixture of rare earth (RE) metals in the proportions in which they are found in the ore from which they are extracted. Although the exact composition of the ore depends on the geographical source, they are all dominated by cerium

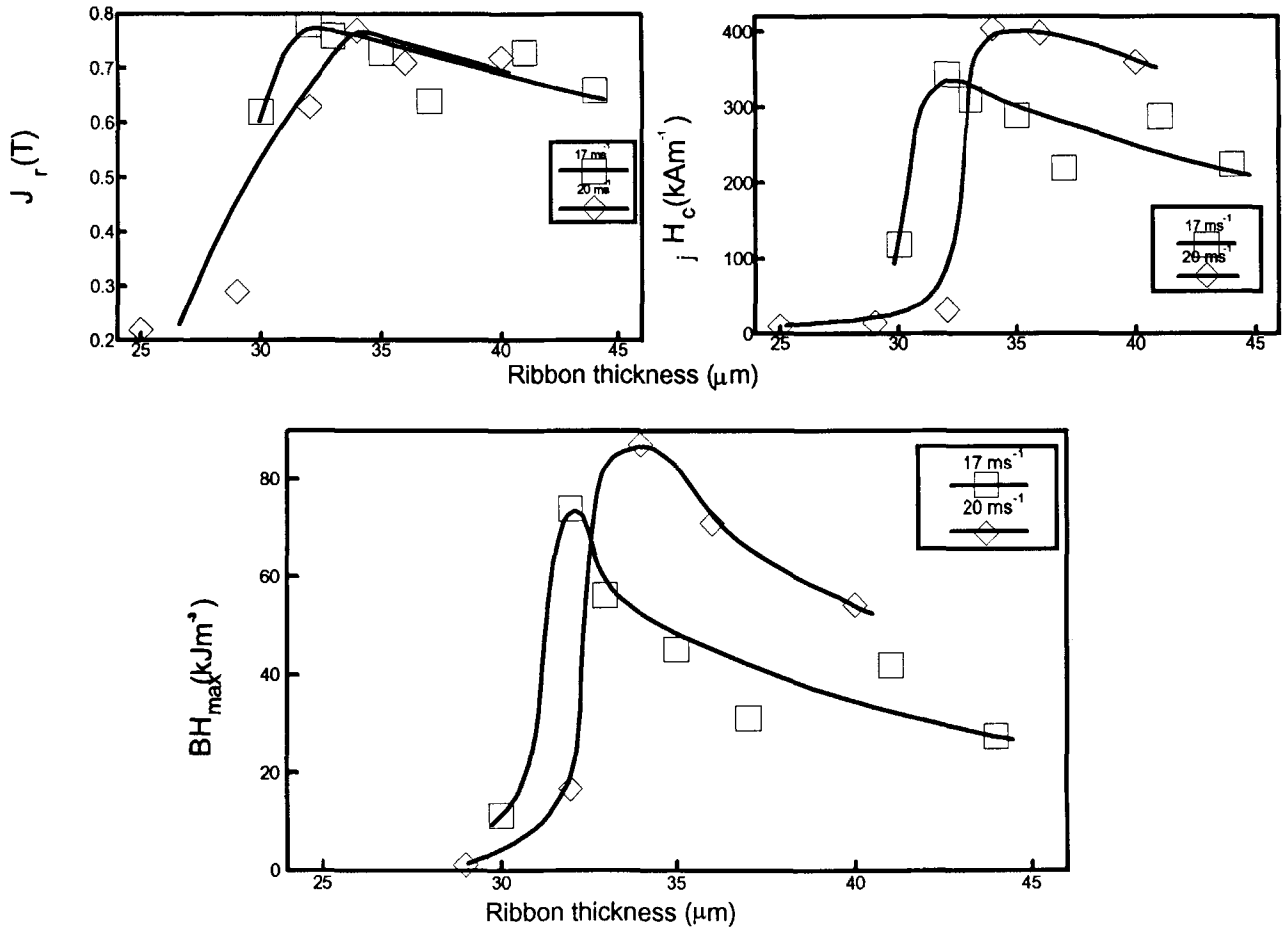

Fig. 11 Dependence of J_r, jH_C, and $(BH)_{max}$ on ribbon thickness for melt-spun ribbon cast at 17 and 20 m · s^{-1} for $Fe_{83}MM_{11}B_6$; the composition of the mischmetal (MM) is given in the text.

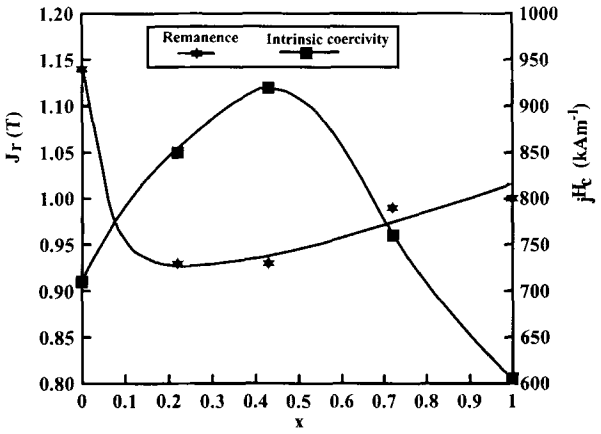

Fig. 12 Variation in the peak values of J_r and $_JH_C$ for ribbons cast at various roll speeds for melt-spun $Fe_{84}(Nd_xPr_{1-x})_{10.6}B_{5.4}$ alloys.

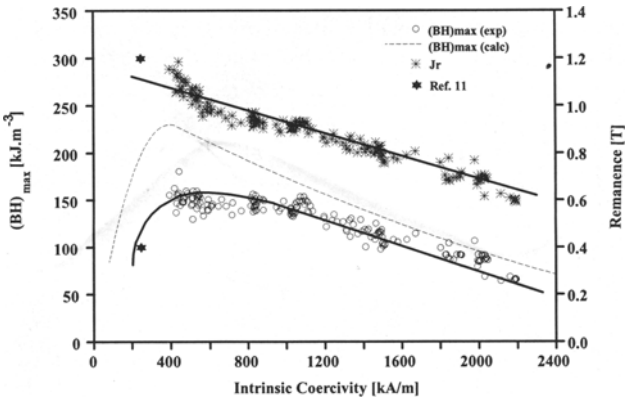

Fig. 13 Experimentally determined J_r versus $_JH_C$ and $(BH)_{max}$ versus $_JH_C$ for a wide range of nanocrystalline and microcrystalline as-spun Fe-Nd-B-base ribbons. Data for $_JH_C < 1600$ kA · m^{-1} typically represent $Fe_{79.6}Nd_{13.2}B_6Si_{1.2}$, whereas those for <500 and >1600 kA · m^{-1} represent alloys of typical compositions $Fe_{85}Nd_9B_6$ and $Fe_{76}Nd_{18}B_6$, respectively. Also shown is the theoretically predicted relationship between $(BH)_{max}$ and $_JH_C$ based on an idealized trapezoidal second quadrant shape.[27]

and lanthanum, which seriously diminish the properties that are useful in permanent magnets based on the tetragonal $RE_{14}Nd_2B$ structure, namely anisotropy field, H_A, Curie temperature, T_c, and J_s.[23] Nevertheless, mischmetal is considerably less expensive than neodymium because the substantial cost of chemically separating similar constituent elements in the former is avoided. The authors have investigated the effects of total substitution of unseparated mischmetal (approximate composition 50% Ce, 23% La, 11% Nd, 6% Pr) for the neodymium in various melt-spun Fe-RE-B alloys.[14] These were shown to have markedly increased J_r when quenched to a nanocrystalline structure, the average grain size being estimated from line broadening analysis (Fig. 11). In the directly quenched state, the best properties obtained for an isotropic ribbon, based on a ternary near-stoichiometric composition $Fe_{83}MM_{11}B_6$, were J_r of 0.78 T and $(BH)_{max}$ of 88 kJ · m^{-3}, compared with 0.60 T and 60 kJ · m^{-3}, respectively, for an alloy with a higher mischmetal concentration, which did not manifest enhanced properties.

In the latter case, for which the structure was microcrystalline rather than nanocrystalline, J_r was in good agreement with a predicted rule of mixtures calculation based on the data for $Fe_{14}RE_2B$ compounds compiled by Livingston.[23] Thus, in spite of the large dilution by cerium and lanthanum, the best J_r and $(BH)_{max}$ for the nanocrystalline $Fe_{83}MM_{11}B_6$ alloy compare quite favorably with those for a microcrystalline $Fe_{14}Nd_2B$ alloy ($J_r \sim 0.8$ T; $(BH)_{max} \sim 110$ kJ · m^{-3}),[1] although the low $_JH_C$ induced by cerium and lanthanum is decreased further by the nanocrystalline structure. Interestingly, however, J_r and $_JH_C$ both increased simultaneously with decreasing ribbon thickness (for constant V_r), in contrast to the FeNdB alloys for which $_JH_C$ was attenuated when J_r was enhanced.

Didymium is a mixture of neodymium and praseodymium, again in the relative proportions in which they coexist in the ore (~3:1 in many ores). Because they are chemically the most similar of the rare earth elements, there is a significant cost benefit in leaving them unseparated, and moreover, $Fe_{14}Nd_2B$ has very similar H_A (at room temperature), T_C, and J_s values to $Fe_{14}Nd_2B$.[23] Again, when spun to the nanocrystalline state, the near-stoichiometric Fe-Nd/Pr-B alloys based on various Nd:Pr ratios showed substantially enhanced J_r (Fig. 12). Taking the peak value of J_r and thus of $(BH)_{max}$ for each Nd:Pr ratio, the best result was obtained for 100% Pr ($J_r \sim 1.4$ T, $(BH)_{max} \sim 176$ kJ · m^{-3}), but the most favorable combination of J_r and $_JH_C$ corresponded to the 75Nd:25Pr ratio, similar to the naturally occurring proportions.

7. Correlation Between Remanence and Coercivity

The remanence is plotted against the corresponding intrinsic coercivity for a wide range of melt-spun FeNdB-base ribbons in the as-cast condition in Fig. 13. These data points represent alloys of various neodymium contents, ranging from 8 to 18 at.% Nd and of widely varying roll speeds, ribbon thickness, and thus mean grain sizes. The low neodymium-containing alloys (8 to 10 at.%), when spun to yield minimum crystallite size (<20 nm), exhibit very high J_r, in excess of 1.0 T, and in some cases up to 1.1 T, but with substantially lowered $_JH_C$, within the range 350 to 500 kA · m^{-1}. For alloys with near-stoichiometric neodymium content (11 to 13 at.%), J_r spans a lower range (0.75 to 1.0 T) for the same spread of grain size, whereas $_JH_C$ is higher (800 to 1200 kA · m^{-1}). The combination of 0.8 T and 1200 kA · m^{-1} is typical for microcrystalline ribbon (grain size ~ 50 nm) having a stoichiometric neodymium content (~12 at.%).

Thus, there appears to be an approximately linear relationship between J_r and $_JH_C$ over a wide range of $_JH_C$, with a general pattern of enhancing one property at the expense of the other. If, for instance, a remanence of 1.0 T was required, then the highest coercivity that could be expected would be ~800 kA · m^{-1}, whereas if a coercivity of 1000 kA · m^{-1} were specified, the maximum remanence possible would be 0.85 T.

The phenomenon of remanence enhancement in the nanostructured materials is believed to result from ferromagnetic exchange coupling between the nanocrystallites, in the absence of a nonmagnetic intergranular phase.[24] In this case, because the exchange field for $Fe_{14}Nd_2B$ greatly exceeds the anisotropy field, spins on atoms adjacent to grain boundaries in favorably oriented crystals are influenced by those in adjacent favorably oriented crystals. Hence, the material can no longer be considered to be an array of noninteracting particles, as is assumed in the Stoner-Wohlfarth model. The smaller the grain size, the greater the intercrystallite boundary area to volume ratio and hence the larger the overall coupling effect. The interaction, however, has an adverse effect on the intrinsic coercivity due to an apparent lowering of the anisotropy energy for the alloy. The influence of enhancing the ratio of the intergranular area to the grain volume on the intergrain exchange interaction in isotropic FeNdB magnets has recently been modeled for 8000 cubic $Fe_{14}Nd_2B$ grains by Fukunaga and Inoue,[25] and this predicts a relationship between reduced remanence and reduced coercivity that bears a close resemblance to that observed in the present experimental investigation (Fig. 13) over the range of J_r relevant here.

It is of interest to observe that, although the low-neodymium alloys (≤10 at.%) contain a soft magnetic secondary phase αFe in addition to the hard $Fe_{14}Nd_2B$ phase, this does not adversely affect the exchange coupling between the $Fe_{14}Nd_2B$ grains. This is considered to be due to the ultrafine particle size of the αFe (typically, ~10 nm), which is smaller than the exchange length for this phase (30 to 40 nm). Consequently, strong interactions are also expected to occur between noncontacting $Fe_{14}Nd_2B$ grains, through the intermediate αFe particles, without inducing a deterioration in the shape of the second quadrant of the *J-H* loop and a resultant collapse in $(BH)_{max}$ that would occur for a coarser (i.e., microcrystalline) grain structure of these two phases. Moreover, because the saturation magnetization J_s of αFe (2.2 T) exceeds that of $Fe_{14}Nd_2B$ (1.6 T), the averaged J_s for the low-neodymium alloys will be higher than that for the stoichiometric composition, and this is considered to contribute in part to the increase in J_r with decreasing neodymium content and hence with progressively increasing volume fraction of αFe phase. This is currently being verified by the current authors through *J-H* loop measurements with maximum fields in excess of H_A for $Fe_{14}Nd_2B$.

A similar behavior to that observed in the present two-phase low-neodymium alloys was reported by Coehoorn et al.[11] in a nanostructured alloy containing only 4 at.% Nd and in which consequently the primary phase was Fe_3B, which is relatively soft magnetically. Although, as indicated in Section 3, only some 15% of the iron atoms were present as the hard magnetic $Fe_{14}Nd_2B$ phase, the nanocrystalline structure (even finer than in the present case) promoted especially strong exchange coupling, to yield a very high remanence of 1.2 T and sufficient hardness to yield an intrinsic coercivity of ~250 kA · m^{-1}.

The influence of a nanocrystalline structure in soft magnetic alloys has recently been the subject of active investigation.[26] A similar exchange coupling effect occurs although, because of the much smaller anisotropy constant that pertains in the soft magnetic alloys, the exchange length is greater than for the present hard alloys. Nevertheless, the result is also a diminishing of the coercivity, although in that case with beneficial effects.

For ribbon of high neodymium-containing (≥13 at.%) alloys, ${}_JH_C$ increases at the expense of J_r, with the latter falling below 0.8 T ($J_s/2$). This results from the presence of a paramagnetic neodymium-rich phase at the grain boundaries, which promotes magnetic isolation of the $Fe_{14}Nd_2B$ crystallites, to increase ${}_JH_C$, but at the same time decreases the volume fraction of the hard phase. Moreover, even when the structure is nanocrystalline, no J_r enhancement occurs because the intercrystalline phase effectively prevents exchange coupling.[22] The higher the neodymium content, the greater the volume fraction of the neodymium-rich phase. Thus, although the J_r-${}_JH_C$ relationship is apparently continuous with that for the stoichiometric and low-neodymium alloys, this is considered to be fortuitous.

8. Effect on Energy Product and Practical Implications for Magnets

The relationship between $(BH)_{max}$ and ${}_JH_C$ for the range of FeNdB-base ribbons currently studied in the as-cast condition is plotted in Fig. 13. It can be seen that $(BH)_{max}$ increases as ${}_JH_C$ decreases below ~1500 kA · m^{-1}, with decreasing grain size, as would be expected from the increasing J_r. However, it begins to level off, in spite of the continually enhancing J_r, toward a maximum of, on average, about 150 kJ · m^{-3} (18.75 MGOe), corresponding to a coercivity of about 450 kA · m^{-1} (although individual values of J_r up to 165 kJ · m^{-3} were observed). Thus, the benefit of increasing J_r as the grain size is increasingly refined is limited by the corresponding decrease in ${}_JH_C$.

Also included in Fig. 13 is a predicted $(BH)_{max}$-${}_JH_C$ relationship, based on an idealized, trapezoidal-shaped second quadrant *J-H* loop shape.[27] This predicts a maximum $(BH)_{max}$ corresponding to ${}_JH_C$ ~ 400 kA · m^{-1}, in close agreement with the current experimental observations. At lower coercivities, $(BH)_{max}$ decreases precipitously, because the BH loop becomes increasingly nonlinear. It is interesting to note that the nanostructured, very low neodymium alloy, $Fe_{77.5}Nd_4B_{18.5}$, investigated by Coehoorn et al.,[11] had such a low coercivity that its $(BH)_{max}$ of 100 kJ · m^{-3} was in fact slightly lower than that of microcrystalline FeNdB, i.e., the $(BH)_{max}$-${}_JH_C$ data point lies on the steeply declining part of the curve. However, it should be noted that this was a three-phase alloy with large volume fractions of the soft phases Fe_3B and αFe.

Clearly, from the practical viewpoint of producing a bonded magnet, it is generally not attractive to have a low coercivity, even though the maximum energy product is substantially enhanced. Thus, it is desirable to compromise somewhat with respect to grain refinement and $(BH)_{max}$ to improve ${}_JH_C$. The dependence of $(BH)_{max}$ on ${}_JH_C$ in Fig. 13 is relatively shallow between 1000 and 450 kA · m^{-1}, and the $(BH)_{max}$/${}_JH_C$ combination of 145 kJ · m^{-3} and 800 kA · m^{-1} represents an excellent compromise.

The discussion so far has centered around the properties of the nanostructured melt-spun ribbons in their as-spun state.

However, the microstructure and magnetic properties of individual ribbon segments are dependent not only on the roll velocity, but also on the local thickness, t_r. For free-jet spinning, it generally is not possible to cast a sizable batch, which would be typical of a commercial operation, within a precise window of thickness, and t_r can vary typically by ±15%. This results in unacceptable microstructure and property variations within the batch and substantial dilution of the $J_r/(BH)_{max}$ enhancement effect. This can, in principle, be overcome by overquenching the alloy into the amorphous state (i.e., to produce a metallic glass) and devitrifying by a controlled anneal to yield a more uniform microstructure. Our recent studies have confirmed the usefulness of this approach, and property combinations of 144 $kJ \cdot m^{-3}$ and 800 $kA \cdot m^{-1}$ have been obtained over a wider range of thickness than is possible by direct quenching.[28] Investigations of the properties of polymer-bonded magnets based on this material are currently in progress.

9. Summary and Conclusions

It is confirmed that, by careful control of spinning conditions, refinement of the grain size in melt-spun FeNdB alloy ribbon containing a small concentration (1.2 at.%) of silicon leads to enhancement of remanence and energy product and that the effect commences at a mean threshold grain size of ~35 nm. The smaller the grain diameter, the greater the improvement in remanence. The phenomenon is thought to result from ferromagnetic exchange coupling between crystallites, which correspondingly reduce the coercivity. The authors' research indicates that the effect, in fact, occurs quite generally for nanostructured iron-rare earth-boron alloys, providing that a paramagnetic iron-rare earth phase is not present. It appears that the latter, which is present in high rare earth content alloys, acts to magnetically decouple the crystallites, but has the effect instead of increasing coercivity. The increase in $(BH)_{max}$ appears to be limited to approximately 160 $kJ \cdot m^{-3}$ for individual FeNdB ribbons, due to the attenuation of coercivity that also results from exchange coupling.

Acknowledgments

The financial support of the Science and Engineering Research Council is gratefully acknowledged. The authors have benefitted from participation in the concerted European Action on Magnets sponsored by the EC.

References

1. J.J. Croat, J.F. Herbst, R.W. Lee, and F.E. Pinkerton, High Energy Product Nd-Fe-B Permanent Magnets, *Appl. Phys. Lett.*, Vol 44, 1984, p 148
2. J.J. Croat, J.F. Herbst, R.W. Lee, and F.E. Pinkerton, Pr-Fe and Nd-Fe-Based Materials: A New Class of High Performance Permanent Magnets, *J. Appl. Phys.*, Vol 55, 1984, p 2078
3. R.W. Lee, E.G. Brewer, and N.A. Schafel, Processing of Neodymium-Iron-Boron Melt Spun Ribbons to Fully Dense Magnets, *IEEE Trans. Magn.*, Vol MAG-21, 1985, p 1958
4. M. Tokunaga, Y. Nozawa, K. Iwasaki, S. Tanigawa, and H. Harada, Magnetic Properties of Isotropic and Anisotropic Nd-Fe-B Bonded Magnets, Rare Earth Permanent Magnets, *Proc. EMRS Symposium*, I.R. Harris, Ed., Amsterdam, North Holland, 1989, p 80
5. R. Bergeron, R.W. McCallum, K. Kanavan, and J.E. Keem, European Patent Application No. 0-195 219 ECD Devices Inc, June 2, 1986
6. G.B. Clemente, J.E. Keem, and J.P. Bradley, The Microstructural and Compositional Influence upon HIREM Behavior in $Nd_2Fe_{14}B$, *J. Appl. Phys.*, Vol 64, 1988, p 5299
7. F. Matsumoto, H. Sakamoto, M. Komiya, and M. Fujikura, Effects of Silicon and Aluminium Additions on Magnetic Properties of Rapidly Quenched Nd-Fe-B Permanent Magnets, *J. Appl. Phys.*, Vol 63, 1988, p 3507
8. G.C. Hadjipanayis and W. Gong, Magnetic Hysteresis in Melt-Spun Nd-Fe-Al-B-Si Alloys with High Remanence, *J. Appl. Phys.*, Vol 64, 1988, p 5559
9. H.A. Davies, K.J.A. Mawella, R.A. Buckley, G.E. Carr, A. Manaf, and A. Jha, Compositional and Process Effects on Structures and Properties of Fe-Nd-B-Based Ribbons and Magnets Produced by the Melt Spinning Route, *Proc. Conf. Concerted European Action on Magnetism*, I.V. Mitchell, Ed., Elsevier Applied Science, London, 1989, p 543
10. K. Yajima, H. Nakamura, O. Kohmoto, and T. Yoneyama, Microstructure of Rapidly Quenched Nd-Fe-Zr-B Magnets, *J. Appl. Phys.*, Vol 64, 1988, p 5528
11. R. Coehoorn, D.B. De Mooij, and C. Dewaard, Melt Spun Permanent Magnet Materials Containing Fe_3B as the Main Phase, *J. Magn. Magn. Mater.*, Vol 80, 1989, p 101
12. A. Manaf, R.A. Buckley, H.A. Davies, and M. Leonowicz, Enhanced Magnetic Properties in Rapidly Solidified FeNdB Based Alloys, *J. Magn. Magn. Mater.*, Vol 101, 1991, p 360
13. A. Manaf, M. Leonowicz, H.A. Davies, and R.A. Buckley, Effect of Grain Size and Microstructure on Magnetic Properties of Rapidly Solidified $Fe_{82.4}Nd_{13.1}B_{4.5}$, *J. Appl. Phys.*, Vol 70, 1991, p 6366
14. S.J. Dobson, R.A. Buckley, and H.A. Davies, "Novel Mischmetal-Iron-Boron and Permanent Magnets Alloys by the Rapid Solidification Route," Proc. 12th Int. Rare Earth and Their Applications, University of West Australia, Canberra, 1992, p 92
15. W.P. Sequeira, S.J. Dobson, R.A. Buckley, and H.A. Davies, Magnetic Properties of Nanocrystalline Melt Spun Iron-Didymium-Boron Alloys, *Mater. Lett.*, Vol 15, 1993, p 376
16. G.E. Carr, H.A. Davies, and R.A. Buckley, Crystallite Size Determinations for Melt Spun Fe-Nd-B Permanent Magnet Alloys, *Mater. Sci. Eng.*, Vol 99, 1980, p 147
17. E.C. Stoner and E.P. Wohlfarth, A Mechanism of Magnetic Hysteresis in Heterogeneous Alloys, *Philos. Trans. Soc.*, Vol A240, 1948, p 599
18. A. Manaf, M. Leonowicz, H.A. Davies, and R.A. Buckley, Nanocrystalline Fe-Nd-B Type Permanent Magnet Materials with Enhanced Remanence, *Mater. Lett.*, Vol 13, 1992, p 194
19. A. Manaf, R.A. Buckley, and H.A. Davies, New Nanocrystalline High Remanence Fe-Nd-B Alloys by Rapid Solidification, *J. Magn. Magn. Mater.*, Vol 12, 1993, in press
20. H.A. Davies, A. Manaf, M. Leonowicz, P.Z. Zhang, S.J. Dobson, and R.A. Buckley, "Nanocrystalline Structures and Enhancement of Remanence and Energy Product in Melt Spun Iron-Rare Earth-Boron Alloys for Permanent Magnets," Proc. 1st Int. Conf. Nanostructured Materials, Cancun, Mexico, Sept 1992, Nanostructured Materials, in press
21. A. Manaf, M. Al-Khafaji, P.Z. Zhang, H.A. Davies, R.A. Buckley, and W.M. Rainforth, Microstructure Analysis of Nanocrystalline Fe-Nd-B Ribbons with Enhanced Hard Magnetic Properties, *J. Magn. Magn. Mater.*, Vol 12, 1993, in press
22. A. Manaf, M. Leonowicz, R.A. Buckley, and H.A. Davies, "High Coercivity Fe-Nd-B Rapidly Solidified Alloys with Additions of Dy, Nb, and Si," Proc. 7th Int. Symp. Magnetic Anisotropy and

Coercivity in Rare Earth Transition Metal Alloys, University of West Australia, Canberra, 1992, p 115

23. J.D. Livingston, "Iron-Rare Earth Permanent Magnets," 8th Int. Workshop on Rare Earth Magnets and Their Applications, K.J. Strnat, Ed., University of Dayton, May 1985, p 423

24. J.E. Keem, G.B. Clemente, A.M. Kadin, and R.W. McCallum, "Magnetism of HIREM Magnets," in Hard and Soft Magnetic Materials with Applications including Superconductivity, Proc. Conf. ASM Materials Week '87, J.A. Salsgiver, Ed., American Society for Metals, 1987, p 27

25. H. Fukunaga and H. Inoue, Effect of Intergrain Exchange Interaction on Magnetic Properties in Isotropic NdFeB Magnets, *Jpn. J. Appl. Phys.*, Vol 31, 1992, p 1347

26. G. Herzer, Grain Size Dependence of Coercivity and Permeability in Nanocrystalline Ferromagnets, *IEEE Trans. Magn.*, Vol 26, 1990, p 1397

27. A. Manaf, P.Z. Zhang, I. Ahmad, H.A. Davies, and R.A. Buckley, "Magnetic Properties and Microstructural Characterisation of Isotropic Nanocrystalline Fe-Nd-B Based Alloys," paper presented at INTERMAG '93, Stockholm, *IEEE Trans. Mag.*, in press

28. P.Z. Zhang, A. Manaf, and H.A. Davies, to be published